

A compact object with a K-type star companion in the solar neighborhood: a wide post-common envelope binary with a white dwarf candidate

JIE LIN,¹ HAILIANG CHEN,^{2,3} BOJUN WANG,⁴ YUDONG LUO,⁵ WENSHI TANG,¹ AND BO HUANG⁶

¹*Department of Astronomy, Xiamen University, Xiamen, Fujian 361005, People's Republic of China*

²*Yunnan Observatories, Chinese Academy of Sciences, Kunming 650216, People's Republic of China*

³*International Centre of Supernovae, Yunnan Key Laboratory, Kunming 650216, P. R. China*

⁴*National Astronomical Observatory, Chinese Academy of Sciences, Beijing 100101, P. R. China*

⁵*School of Physics, Peking University, and Kavli Institute for Astronomy and Astrophysics, Peking University, Beijing, 100871, China*

⁶*Institut de Ciències de l'Espai (ICE-CSIC), Campus UAB, Can Magrans S/N, E-08193 Cerdanyola del Vallès, Catalonia, Spain*

ABSTRACT

Post-common envelope binaries (PCEBs) consisting of a white dwarf (WD) plus a main-sequence (MS) star can constrain current prescriptions of common envelope evolution (CEE) and calibrate theoretical models of binary formation and evolution. Most PCEBs studied to date have typical orbital periods of hours to a few days and can be well explained by assuming inefficient CEE to expel the envelope. However, there are currently several systems with relatively wide orbital periods (>18 days). To explain these wide PCEBs, additional sources of energy have been suggested to be taken into account. Here, we present the discovery and observational characterization of a compact object ($M \geq 0.58 M_{\odot}$) with a K-type star companion in the solar neighborhood ($d \sim 112$ pc) and an orbital period of $P_{\text{orb}} \sim 14$ days. The compact object binary is likely to be a system consisting of a WD and a barium dwarf. Such a system with an orbital period within the gap between tight and wide binaries provides a test of whether additional energy sources are required to explain its formation. Using binary evolution models, we investigate the evolutionary history of this wide PCEB system and find that the observed properties of this source can be explained without invoking any extra energy source.

Keywords: binaries: spectroscopic – stars: compact object – stars: evolution – white dwarfs

1. INTRODUCTION

Common envelope evolution (CEE) is one of the major unsolved problems in modern astronomy and astrophysics. CEE is formed when a giant donor star overflows its Roche lobe, typically as a consequence of dynamically unstable mass transfer. During CEE, angular momentum and orbital energy are extracted from the orbit to eject the envelope. If the envelope is successfully ejected, a close binary containing a compact object and its main-sequence (MS) companion will be left. If the envelope is not successfully ejected, the CEE will lead to the merger of the binary system. Modeling of CEE is an important progress towards the understanding of the formation of a wide variety of compact binary systems, such as cataclysmic variables (Paczynski 1976; Warner 1995), X-ray binaries (Kalogera & Webbink 1998), double-degenerate binaries (Webbink 1984), binary neutron stars (Bhattacharya & van den Heuvel 1991), and binary black holes (Belczynski et al. 2016). Due to the complex physical processes involved in the CEE, simplified models of CEE based on energy or angular momentum conservation are commonly used in terms of modeling the evolution of large numbers of binaries and understanding the possible formation pathways of individual system.

In current binary evolution models, CEE is commonly approximated by a parametrized energy equation, i.e. a fraction of the liberated orbital energy, known as the common envelope (CE) efficiency (α_{CE}), is equal to the binding energy of the envelope to determine the post-CEE orbital separation (Paczynski 1976; Warner 1995; Iben & Tutukov 1986; Iben & Livio 1993). This model has been calibrated by comparing the predicted binary populations with the

abundance of observed post-common envelope binaries that contain white dwarfs (WDs). Previous modeling attempts to reconstruct the CE phase for observed post-common envelope binaries (PCEBs) and empirically constrain α_{CE} . Several calculations have found that the vast majority of systems, with typical orbital periods of hours to a few days, can be best reproduced by assuming inefficient CE evolution with $\alpha_{\text{CE}} \sim 0.25$ (Zorotovic et al. 2010). However, it remains unclear whether additional energy sources play an important role in unbinding the envelope for wide PCEBs. One notable example is IK Peg (Wonnacott et al. 1993), a 22-days binary containing a massive WD ($1.19 M_{\odot}$), whose orbit can only be explained when additional energy sources, such as the recombination energy of hydrogen and helium released in the expanding envelope of the WD progenitor, are included in the energy budget (Davis et al. 2010; Zorotovic et al. 2010). In addition, several wide WD + MS binaries with orbital periods from a few tens to a few hundreds of days have been discovered via *Kepler* survey and *Gaia* Data Release 3 (DR3) catalogue (Kruse & Agol 2014; Kawahara et al. 2018; Yamaguchi et al. 2024). These long-period PCEBs, such as IK Peg, cannot be explained by classical CE evolution without contributions from additional energy sources in the CE energy balance. However, the formation of long-period PCEBs may remain if mass transfer begins during a thermally-pulsing asymptotic giant branch (TP-AGB) phase of the donor star (Belloni et al. 2024). According to this formation scenario, the slow neutron-capture (*s*-process) elements were transferred to the main-sequence stars from a more evolved companion when the latter was in its TP-AGB phase (McClure et al. 1980). This can result in an overabundance of barium and other *s*-process elements on the surface of the main-sequence stars, which are historically known as Barium stars.

Large spectroscopic surveys, such as the Large Sky Area Multi-Object Fiber Spectroscopic Telescope (LAMOST) and the *Gaia* mission, have observed millions of stars and build extensive spectroscopic databases. Radial-velocity modulation detected in optical spectra offer a promising method for identifying unseen compact objects in binary systems with stellar companions. These databases open a new opportunity to search for black holes (BHs), neutron stars (NSs), and long-period PCEBs binaries with massive WD (Ren et al. 2020; Yuan et al. 2022; Yi et al. 2022; Zheng et al. 2022; El-Badry et al. 2023a,b; Lin et al. 2023; Qi et al. 2023; Zhao et al. 2024; Gaia Collaboration et al. 2024; Liu et al. 2024; Yamaguchi et al. 2024).

In this article, we report a single-lined binary consisting of a K-type main-sequence star and a compact object, which is likely a long-orbital-period PCEB composed of a WD and a barium dwarf. The paper is organized as follows. The identification of a wide PCEB with WD candidate from the catalog of *Gaia* DR3 single-lined spectroscopic binaries (SB1s) is described in Section 2. The data analysis and the result are presented in Section 3. Section 4 discusses the possibilities for the nature of unseen companion and presents models of WD progenitors and constraints on CEE. Our conclusions are presented in Section 5.

2. DISCOVERY

Gaia DR3 provides orbital solutions for more than 181000 single-lined spectroscopic binaries (SB1s), enabling the identification of candidate systems that may host compact object companions such as WDs, NSs, or BHs (Gaia Collaboration et al. 2023). Furthermore, the Fourth *Fermi* Large Area Telescope Source Catalog (4FGL) DR3 contains more than 2000 unassociated γ -ray sources, representing potential reservoirs harboring a significant population of undiscovered spider pulsar binary systems (e.g. Lin et al. 2024). In this project, we performed a cross-match between *Gaia* DR3 SB1s and the 4FGL-DR3 catalog, selecting systems exhibiting significantly large mass functions in their *Gaia* DR3 radial velocity (RV) solutions to search for spider pulsar binary system candidates. We discovered a candidate with the optical source of *Gaia* DR3 located at R.A.(J2000) = $04^{\text{h}}47^{\text{m}}28^{\text{s}}.48$ and Decl.(J2000) = $+24^{\circ}44'52.^{\prime\prime}4$, inside the 95 % error region of the γ -ray source 4FGL J0447.2+2446 (See Fig 1).

In *Gaia* DR3, the source_id of J0447 is 147167226196998272 with a bright ($G=11.95$) K-type main-sequence star. Its DR3 parallax of $\omega_{\text{DR3}} = 8.96 \pm 0.04$ mas implies a distance of $d \sim 112$ pc. The RV solution of *Gaia* DR3 gives the orbital period ($P_{\text{orb}} = 13.396 \pm 0.002$ days), eccentricity ($e = 0.03 \pm 0.01$), semi-amplitude ($K = 42.37 \pm 0.53 \text{ km s}^{-1}$) and center-of-mass velocity ($\gamma = 59.20 \pm 0.36 \text{ km s}^{-1}$). For γ -ray source 4FGL J0447.2+2446, its γ -ray spectrum can be fitted with a logParabola model (Abdollahi et al. 2022). 4FGL J0447.2+2446 has a 0.1–100 GeV flux of $(4.19 \pm 0.73) \times 10^{-12} \text{ erg s}^{-1} \text{ cm}^{-2}$, corresponding to a luminosity of $L_{\gamma} = (6.3 \pm 1.1) \times 10^{30} \text{ erg s}^{-1}$ at a fiducial distance of 112 pc. This estimated γ -ray luminosity of J0447 is far less than within the range of luminosities (4×10^{32} – $4 \times 10^{34} \text{ erg s}^{-1}$) of the spider pulsar family. Notably, PSR J0447+2447 is spatially coincident within the 68 % confidence level with the γ -ray source 4FGL J0447.2+2446 (See Fig 1). This suggests that the *Gaia* source is likely a chance alignment with the gamma-ray source, which has a different more likely counterpart. PSR J0447+2447 is an isolated millisecond pulsar (MSP) with a spin period of 2.99 ms and a dispersion measure (DM) of $32.907 \text{ cm}^{-3} \text{ pc}$

(Wu et al. 2023). For PSR J0447 + 2447, the distance of 0.92 kpc derived from the YMW16 model (Yao et al. 2017) corresponds to a gamma-ray luminosity of $L_\gamma = (4.28 \pm 0.75) \times 10^{32}$ erg s $^{-1}$, which lies within the characteristic range for millisecond pulsars. Therefore, 4FGL J0447.2+2446 is essentially the γ -ray counterpart of the PSR J0447+2447 rather than J0447. However, the possibility that the observed γ -ray flux originates from multiple sources cannot be entirely excluded, since two counterparts lie within the 95% confidence level. Hence, multi-wavelength observations are required to determine the nature of invisible star in J0447.

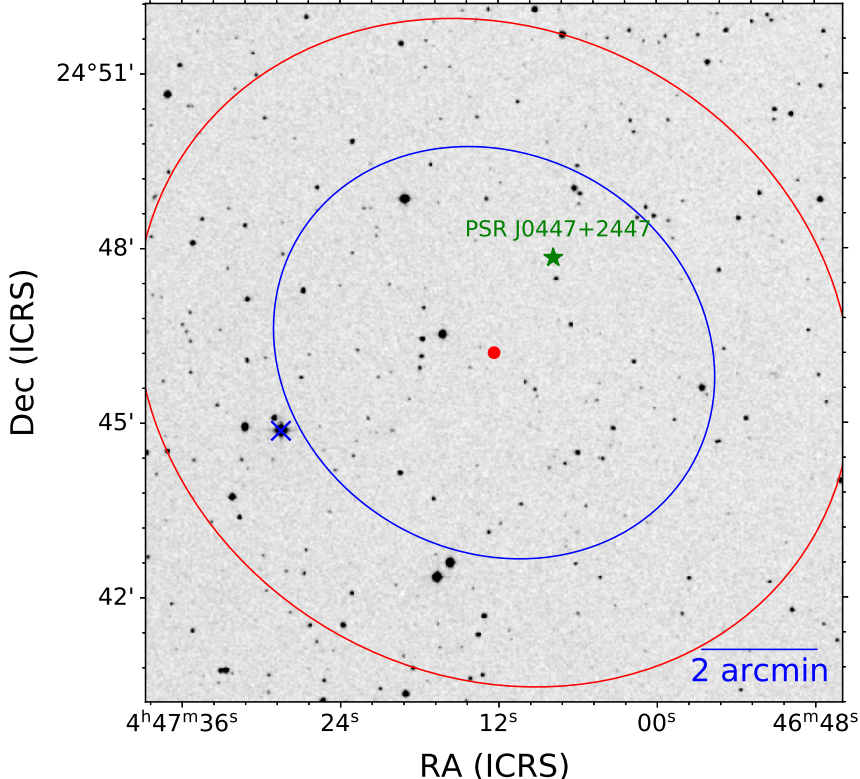


Figure 1. The Digitized Sky Survey (DSS) image of the 4FGL J0447.2+2446. The red and blue ellipses show 68% error ellipse and 95% error ellipse of 4FGL catalog, respectively. The PSR J0447+2447 (green star) is localized within the 68% confidence level of 4FGL J0447.2+2446, while the optical source (blue cross) position is contained in the 95% confidence region.

3. DATA ANALYSIS AND RESULTS

3.1. Optical Photometry

The ZTF DR23 archive¹ contains about five hundred brightness measurements of J0447 in the g band covering about 6.6 yr (MJD 58204–60609). We use the Lomb-Scargle method Lomb (1976); Scargle (1982), to search for periodic brightness variations in the range of 0.01–30 days. The resulting periodogram is shown in the upper panel of Fig. 2. No periodic signals exceeding the 2σ confidence level were detected in the periodogram. The blue dashed lines in the plot represent the 2σ confidence level.

In addition, we retrieved photometry of the source in *Gaia* DR3 (G , G_{BP} , and G_{RP}), 2MASS (J, H and K_s), SDSS (u), WISE (W1 and W2) and *TESS* (T), and fit the spectral energy distribution (SED) with the astroARIADNE² (spectralAeneRgy dIstribution bAyesian moDel averagiNg fittEr Vines & Jenkins 2022). The SED fit yields $T_{\text{eff}} = 4568^{+15}_{-11}$ K,

¹ <https://irsa.ipac.caltech.edu/cgi-bin/Gator/nph-dd>

² <https://github.com/jvines/astroARIADNE>

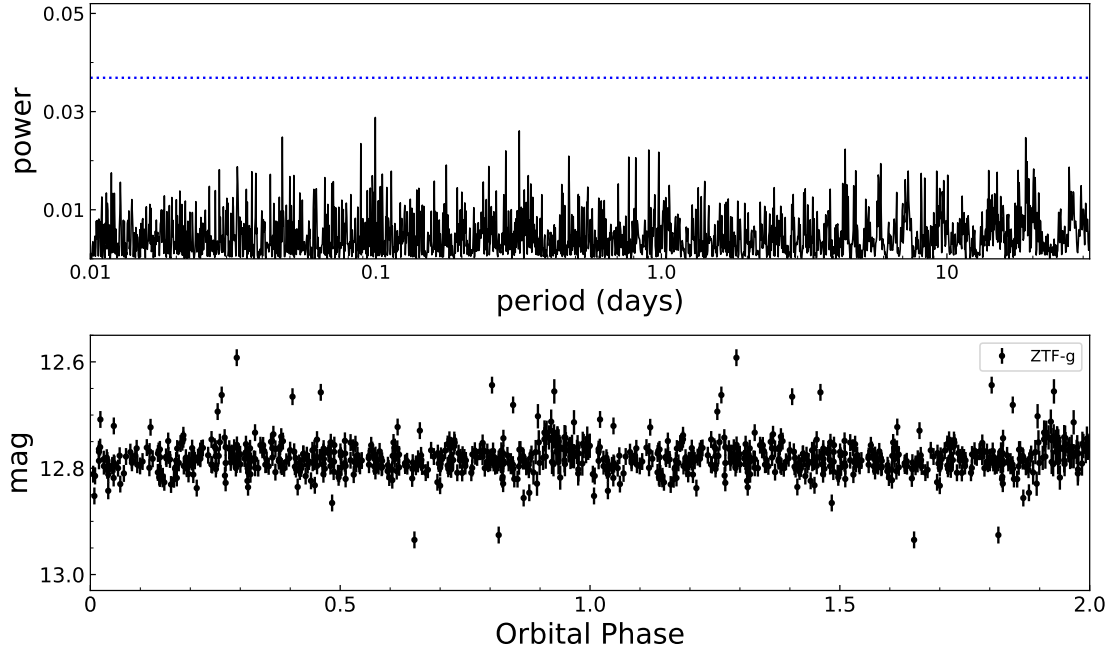


Figure 2. Top panel shows the Lomb-Scargle periodogram of the complete ZTF dataset (MJD 58204-60609), with dashed horizontal line is the 95% confidence limits. Bottom panel shows the ZTF light curves folded at the orbital phase derived from LAMOST RV measurements.

$R = 0.690^{+0.006}_{-0.006} R_{\odot}$ by using the extinction value of $A_v = 0$ derived from three-dimensional dust maps (Green et al. 2019), where A_v is the extinction measured in the V band. We find that the source is well fit by a single-star model (See Fig. 3), which suggests that the invisible star of J0447 is likely a compact object. The astroARIADNE code gives a mass of $M_K = 0.70 \pm 0.04 M_{\odot}$ using the stellar evolution model (isochrones). Based on the mass-luminosity relations from Mann et al. (2019), we obtain the result that the visible star has a mass of $0.68 \pm 0.02 M_{\odot}$, which is consistent with the one from the stellar evolution models.

3.2. Optical Spectroscopy

To further validate the orbital solution of the *Gaia* DR3, we searched for archived data from other telescopes. The source was also observed by the LAMOST survey. We obtained 3 low-resolution spectra (LRS) from December 2012 to January 2019, covering a wavelength range from 369 nm to 910 nm (Luo et al. 2015), and 46 medium-resolution spectra (MRS) from November 2017 to October 2018, with the blue and red arms covering wavelength ranges from 495 nm to 535 nm and from 630 nm to 680 nm, respectively. The low- and medium-resolution spectra have spectral resolution $R \sim 1800$ and $R \sim 7500$, respectively. We derived the barycentric velocity of each spectrum through the cross-correlation technique. In addition, the optical spectroscopy of LAMOST also presents a single-line binary (one visible star only). For 4 MRS, we use the spectra of the blue arms to measure radial velocities. The cross-correlation has been performed using the spectral template ($T_{\text{eff}} = 4568$ K, $\log g = 4.56$, $[\text{Fe}/\text{H}] = -0.28$) calculated with the MARCS model (Gustafsson et al. 2008). The RV was obtained and we fit our radial-velocity data using the custom Markov Chain Monte Carlo sampler TheJoker (Price-Whelan et al. 2017). The best-fitting parameters with 1σ uncertainties are period $P_{\text{orb}} = 13.3968 \pm 0.00058$ days, semi-amplitude $K = 44.11 \pm 2.57 \text{ km s}^{-1}$, eccentricity $e = 0.05 \pm 0.02$, and center-of-mass velocity $\gamma = 53.78 \pm 1.37 \text{ km s}^{-1}$. This orbital solution also agrees with *Gaia* DR3.

To derive the surface gravity and metallicity of the K-type star, we use the spectral synthesis codes iSpec (Blanco-Cuaresma et al. 2014; Blanco-Cuaresma 2019). iSpec generates synthetic spectra based on the SME (Piskunov & Valenti 2017) and MARCS (Gustafsson et al. 2008) model atmospheres and outputs the best-fitting stellar parameters using a χ^2 minimization process. This fits yield $T_{\text{eff}} = 4620 \pm 70$ K, $\log g = 4.48 \pm 0.17$, and $[\text{Fe}/\text{H}] = -0.41 \pm 0.07$ (See Fig 5.). This result is consistent with the previous SED fitting within the uncertainty. We compared the spectrum of J0447 to spectra of another star with similar stellar parameters and abundances observed by the LAMOST survey. The two spectra are very similar, which also suggest that the invisible companion of J0447 is a compact object.

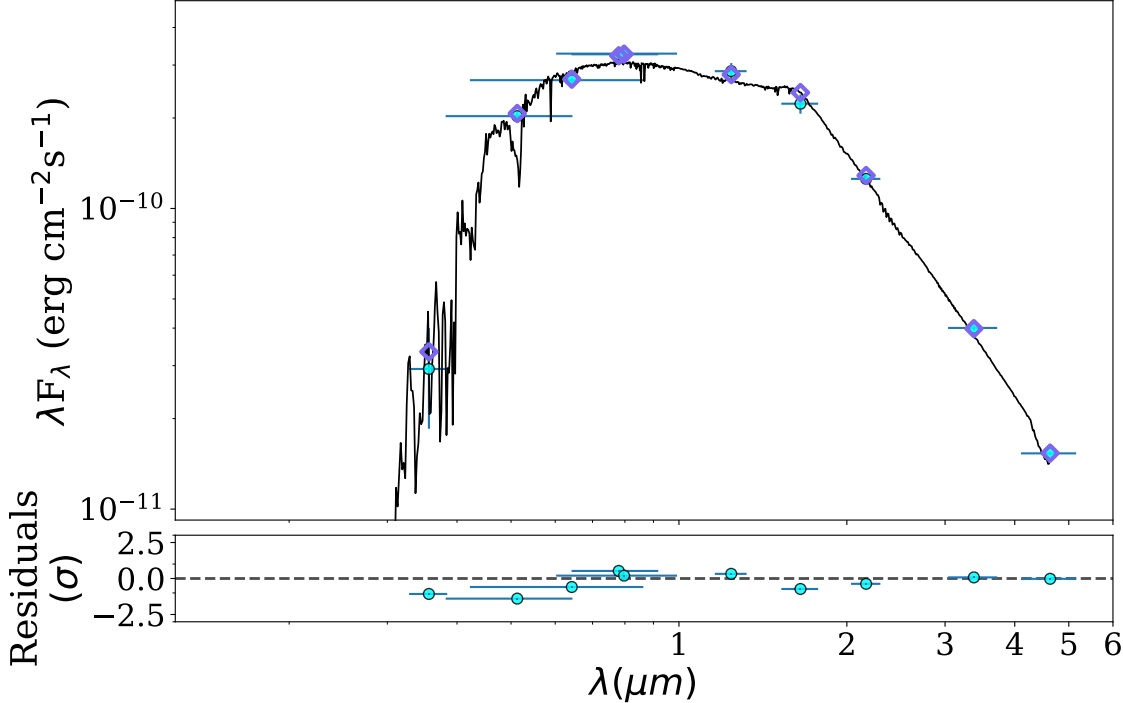


Figure 3. The best-fitting SED model for J0447 after fixing the extinction parameters $A_v = 0$. The black curve is the best-fitting model. The green pluses and circles are for the retrieved photometric measurements, while the blue diamonds are for synthetic photometry.

Notably, the K-type star presents an overabundance of *s*-process elements (such as Sr, Ba and La) in low-resolution spectra from LAMOST using the data-driven Payne method (Xiang et al. 2019; Zhang et al. 2025). In addition, Song et al. (2024) uses the memory-enhanced adaptive spectral network (MEASNet) to search for barium star candidates in the LAMOST low-resolution survey and estimates the abundance of five *s*-process elements of the K-type star: [Ba/Fe]=0.86, [Ce/Fe]=0.50, [Nd/Fe]=0.22, [Sr/Fe]=0.28 and [Y/Fe]=0.37³. Therefore, the K-type star of J0447 is likely a barium dwarf that was contaminated by an AGB companion. However, high-resolution spectroscopic observations should be required to further confirm the nature of the K-type star.

3.3. Radio observation and pulse search

We observed J0447 using FAST on August 13, 2024 and March 2, 2025 (Obs. IDs: PT2024_0156 and PT2024_0133; PI: Jie Lin). The integration times were 1200 s and 3000 s, respectively. Observations employed the Pulsar Search Tracking Mode with the central beam of the 19-beam receiver (Jiang et al. 2020), covering 1.0–1.5 GHz through 4096 channels. Data were recorded with temporal resolution of 49.152 μ s and full Stokes polarization.

We searched for both periodic signal and single pulses using PRESTO (Ransom 2001) and TransientX (Men & Barr 2024), respectively. For periodic searches, RFI mitigation was performed with RFIFIND provided by PRESTO. The dispersion measure (DM) search range was 0–30 pc cm⁻³, and the upper limit significantly exceeds the DM value predicted by the YMW16 (Yao et al. 2017) Galactic electron-density model at a distance of 112 pc. We performed the Fourier-domain acceleration search by adopting $z_{\text{max}}=10$. No periodic radio pulsation was found in either observations. The DM range for single-pulse searches was identical to that used for the periodic search. No significant single-pulse was detected above $S/N = 7$. By applying the radiometer equation, we estimate a flux density upper limit $S_{\text{min}} = 2.52 \mu\text{Jy}$ at 1.25 GHz for the 3000 s observation, assuming $S/N_{\text{min}} = 5$ and a 20% duty cycle.

3.4. Mass of the unseen companion

³ doi:10.5281/zenodo.12618383

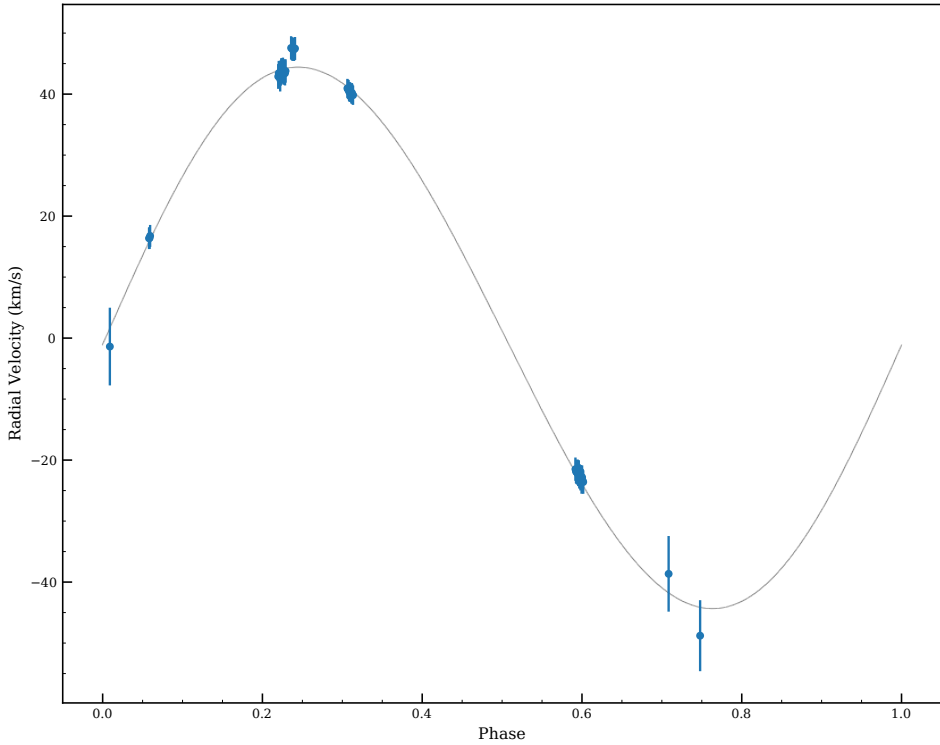


Figure 4. The observed RVs of J0447, measured at 49 orbital phases from LAMOST low- to medium-resolution spectra, are plotted as a function of orbital phase with the best-fitting RV curve overlaid.

From the resulting RV parameters, we calculate the mass function $f(M)$:

$$f(M) = \frac{P_{\text{orb}} K^3 (1 - e^2)^{3/2}}{2\pi G} = \frac{M_C^3 \sin^3 i}{(M_C + M_K)^2}, \quad (1)$$

where M_C and M_K are the masses of the invisible companion and K-type star, respectively. We find $f(M) = 0.12 \pm 0.02 M_{\odot}$. The mass of the K-type star, $M_K = 0.70 \pm 0.04 M_{\odot}$, was derived from the stellar evolution model. Given the mass function and the mass of the K-type star, the mass of the invisible companion still remains unconstrained due to the lack of inclination i . However, the light curve of J0447 does not exhibit significant ellipsoidal variability, preventing constraints on inclination i . Therefore, we can only place a lower limit on the invisible companion mass when $i = 90^\circ$. The derived mass for the invisible companion is $M_C \geq 0.58 \pm 0.05 M_{\odot}$.

The mass of the invisible companion, M_C , as a function of the inclination is shown in Fig. 6, adopting $M_K = 0.70 M_{\odot}$. The integrated probability of inclination i can be calculated as $\cos i$ under the assumption of randomly oriented orbital planes. The probability of the invisible companion being a white dwarf, neutron star or black hole is about 82%, 10% and 8%, respectively. Therefore, the invisible companion is likely a white dwarf.

4. DISCUSSION

4.1. MS companion

The luminosity of MS companion with a mass of $M_C \geq 0.58 \pm 0.05 M_{\odot}$ is almost consistent with the K-type star. The medium-resolution spectra from LAMOST have already covered the semi-amplitude phase of the RV curve. Therefore, in this case, the LAMOST spectra are sufficient to reveal two sets of spectral lines and the variations in the composite line profiles with orbital phase. In addition, the spectra of J0447 are well fitted by single-star models and

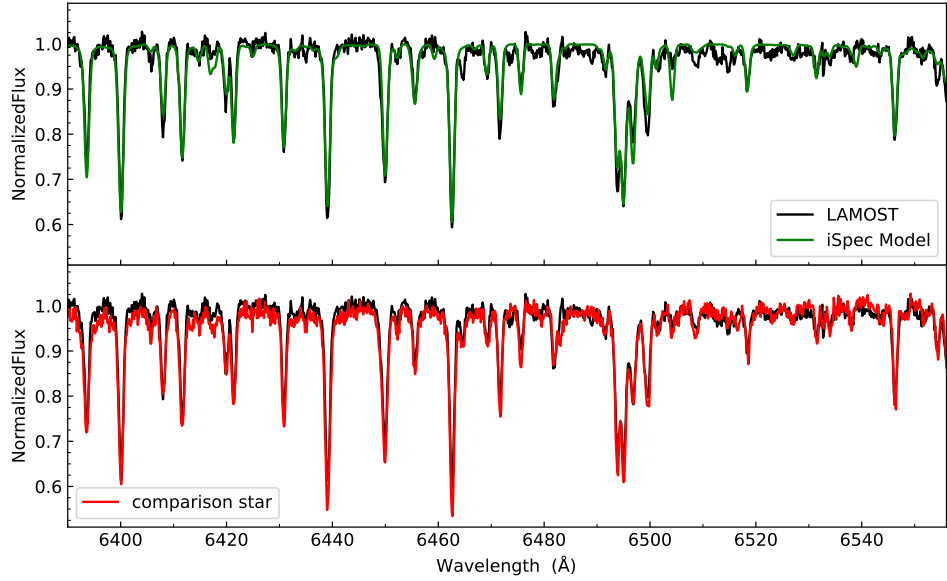


Figure 5. The top panel displays a synthetic model spectrum (green) in the red arms, generated using atmospheric parameters derived from iSpec. The bottom panel compares the spectrum of J0447 with that of a comparison star (red) observed by LAMOST, which has similar stellar parameters and chemical abundances. The spectral similarity rules out significant light contamination from a companion.

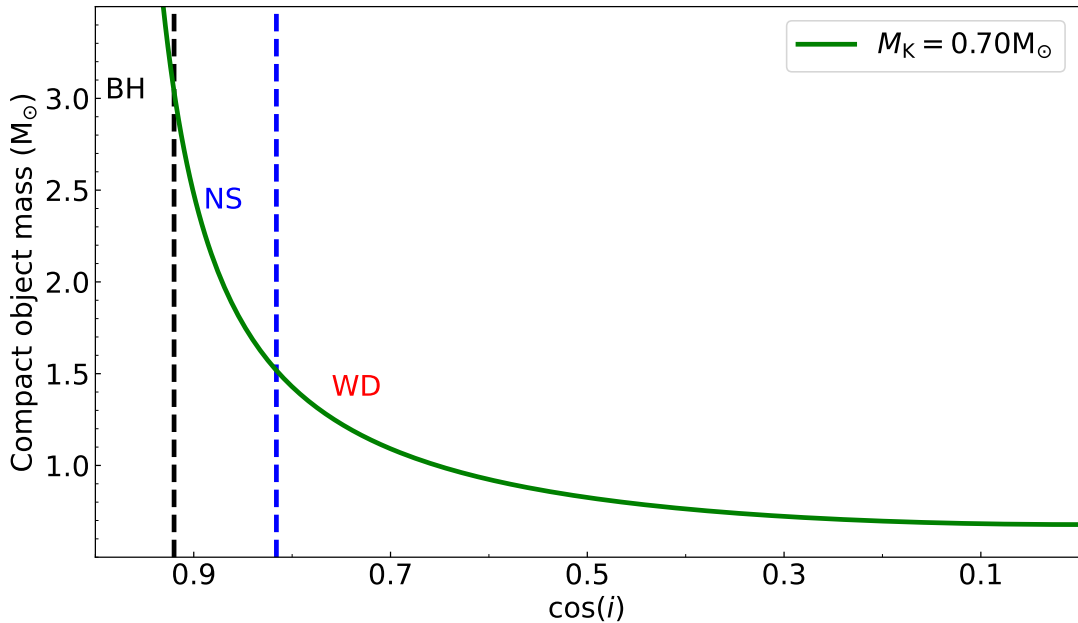


Figure 6. Plots of the unseen companion mass as a function of inclination, i , on the basis of the measured mass function for $0.7\text{-}M_{\odot}$ K-type star. Assuming that the orbital plane is randomly distributed, the integrated probability of inclination angle can be calculated as $\cos(i)$.

are consistent with those of single stars observed by LAMOST. Therefore, the presence of a main-sequence companion can be definitively ruled out.

4.2. Neutron star or black hole

Due to the lack of constraints on the orbital inclination, only the minimum mass of the unseen companion can be determined. Therefore, we also consider the possibility that the unseen companion is a NS or a BH, particularly given that this compact binary system resides as close as ~ 100 pc from Earth. Over the past two decades, many experiments have detected pulses of radionuclide ^{60}Fe in deep-sea deposits between 2 and 3 Myr ago (Knie et al. 1999; Wallner et al. 2016). In addition, there are measurements of ^{60}Fe in the lunar regolith (Fimiani et al. 2016), in cosmic rays (Binns et al. 2016), and in Antarctic snow (Koll et al. 2019). The discovery of these live radioactive isotopes is believed to be recent astrophysical explosions such as core-collapse supernovae (CCSN) within ~ 100 pc of Earth. If the unseen companion is indeed a NS or BH, it will be the nearest NS or BH. Furthermore, we performed a kinematic analysis of J0447's orbit in the galaxy using the *Gaia* astrometric solution and the systematic RV and found that it can pass through our solar neighborhood spanning the past 2-3 Myr (See Fig 7.). This may suggest that the radionuclide ^{60}Fe signal is associated with its CCSN event.

Either NSs or BHs are expected to receive natal kicks that impart eccentricity to their orbits. In the specific case where the natal kick arises solely from spherically symmetric mass loss and the pre-supernova orbit is circular (Blaauw 1961), the resulting eccentricity e is given by

$$e = \frac{\Delta M}{M_c + M_2}, \quad (2)$$

where ΔM is the mass lost during the supernova, M_c is the mass of the resultant compact object (NS or BH), and M_2 is the mass of the companion star. For an NS formed in this scenario, we consider a 8-M_\odot star undergoing an ultra-stripped core-collapse SN with $\sim 0.3\text{-M}_\odot$ ejecta (De et al. 2018; Yao et al. 2020), forming a typical 1.4-M_\odot NS around a 0.7-M_\odot MS companion. The resulting eccentricity ($e \sim 0.14$) is significantly larger than the system of J0447. Asymmetric supernovae can impart strong natal kicks to NSs, generating even higher eccentricities than those produced by spherically symmetric mass loss alone. Consequently, the highly circular orbit of J0447 is difficult to reconcile with the mechanisms of NS formation. Furthermore, deep FAST radio observations reveal no radio pulsed signals when ignoring unfavorable beaming geometries. This further strengthens the evidence that the unseen companion is unlikely to be an NS.

On the other hand, if the unseen companion is a BH and the natal kick was purely due to mass loss during its formation, the orbital eccentricity ($e \sim 0.05$) of the system can place a constraint on the mass of the BH. Assuming a minimum mass loss of $\sim 0.3\text{-M}_\odot$, a BH mass of $M_{\text{BH}} \geq 5.3\text{ M}_\odot$ would be required to fully account for the observed eccentricity. For a random distribution of the orbital inclination angle, the probability of obtaining such a low inclination angle ($\sim 18^\circ$) is less than 5% since the BH mass exceeds 5.3 M_\odot . Furthermore, if the SN is asymmetric, imparting an additional kick on the BH, this would likely result in a higher BH mass and a concomitantly lower probability of having a low inclination angle, as the kick contributes additional eccentricity to the system. Although the possibility that the unseen companion is an NS or BH cannot be entirely ruled out, it appears highly unlikely. Therefore, the unseen companion is likely a WD, and we proceed under this assumption.

4.3. A white dwarf in post-common envelope binaries

We identified a close binary star consisting of a K-type star and most likely a WD. Only a minimum mass of the unseen companion is obtained due to the lack of inclination angle. In what follows, we compare the properties of our targets with other related classes of binaries and investigate possible implications for WD binary formation and evolution by reconstructing their past.

4.3.1. A population of PCEBs in the literature

The Sloan Digital Sky Survey (SDSS) efficiently identifies substantial populations of close white dwarf–main-sequence (WDMS) binaries (Abazajian et al. 2009; Rebassa-Mansergas et al. 2007). Zorotovic et al. (2010) compiled a sample of 60 PCEBs, comprising 35 systems newly identified through the Sloan Digital Sky Survey (SDSS) and 25 previously known systems. In addition, the “white dwarf binary pathways survey” also identified some PCEBs that consist of a WD plus an intermediate mass companion star of spectral type AFGK (Hernandez et al. 2021, 2022a,b). With the exception of the IK Peg system (~ 21.7 days), the orbital periods of all other systems are less than 10 day. Beyond

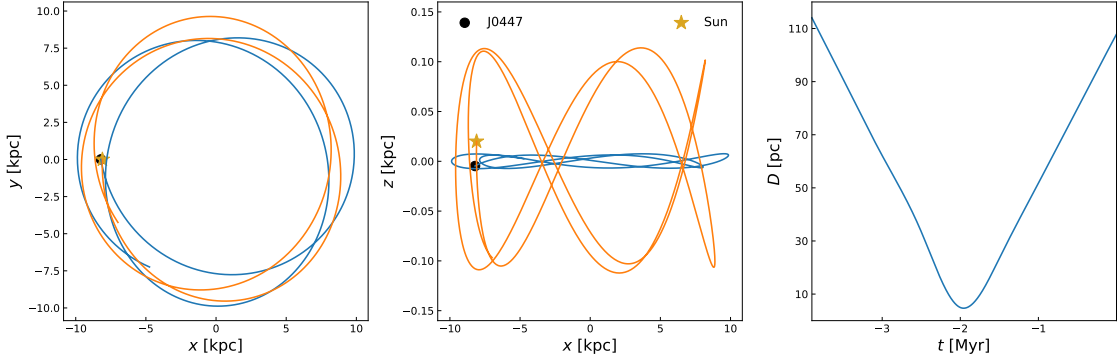


Figure 7. Left-hand and middle panels show the Galactic xy-plane and xz-plane orbital projections of J0447 and the Sun, respectively, calculated via 500 Myr backward integration from the measured proper motion and centre-of-mass RV (Price-Whelan 2017). Right-hand panel shows the temporal evolution of the distance between J0447 and the Sun over past several Myrs.

IK Peg, multiple long-period white dwarf–main-sequence self-lensing binaries (SLBs) have been identified through systematic pulse surveys in the Kepler light curves (Kruse & Agol 2014; Kawahara et al. 2018). More recently, Yamaguchi et al. (2024) identified five PECBs hosting massive WD candidates paired with main-sequence companions of spectral types earlier than M. These systems exhibit long orbital periods (18–49 days) derived from spectroscopic and astrometric data – classified as SB1 or astrometric + spectroscopic (AstroSpectroSB1) in the *Gaia* DR3. As illustrated in Figure 8, only three self-lensing binaries (SLBs) reside near the P - M_{wd} relation for WDs, whereas the remaining sample systems deviate significantly from this trend (Lin et al. 2011). This deviation indicates that the outliers likely formed through common-envelope evolution (CEE) rather than stable Roche-lobe overflow (RLOF). The three SLBs exhibit long orbital periods and near-circular orbits, consistent with formation via stable mass transfer from an evolving primary – a mechanism analogous to that observed in field and open-cluster blue stragglers (Kawahara et al. 2018).

For PCEBs with orbital periods less than 10 days, Zorotovic et al. (2010) demonstrated that all known systems can be reconstructed using a relatively low CE efficiency ($\alpha_{\text{CE}} \sim 0.25$), indicating inefficient orbital energy transfer during envelope ejection. In contrast, there are currently several PCEB systems with long orbital periods that range from a few tens to a few hundreds of days. It has been claimed that these systems cannot be explained by CEE without contributions from recombination energy. However, Belloni et al. (2024) argued that extra energy is not required to explain PCEB systems with long orbital periods when the WD progenitor have to be highly evolved TP-AGB star at the onset of the CE evolution. However, it remains to be observationally tested whether all wide-orbit systems necessarily evolve into highly evolved TP-AGB stars before CE evolution. If so, the heavy s -process elements, such as Ba, La, or Ce, and light s -process elements, such as Sr, Y, or Zr, might be detectable in the spectra of some companion stars (Escorza & De Rosa 2023). Interestingly, the low-resolution spectra from LAMOST indicates potential s -process element enrichment in the K-type star of our target, suggesting that the WD progenitor likely went through the TP-AGB phase.

4.3.2. The evolutionary history of J0447

From the previous section, we know that the MS donor is populated by the s -process elements, which are produced from TP-AGB star. This means that the progenitors of the WDs should undergo TP-AGB phases. Assuming that the compact object is a WD, the formation scenario of the J0447 system is as follows. In a main-sequence binary, the primary evolves to the TP-AGB phase and fills its Roche lobe, while the secondary is still a main-sequence star. Then the system experiences an unstable mass transfer and enters the common envelope phase. After the ejection of the CE, the system evolves into a binary system consisting of a WD and a MS star. Below we try to constrain the binary parameters of the progenitors of J0447.

For a binary system to enter a CE phase, the mass ratio must exceed a critical mass ratio. In this case, we refer to the critical mass ratio given by Hurley et al. (2002) (see their Eq. 57). For the common envelope process, we adopt the energy budget prescription, i.e.

$$\alpha_{\text{CE}} \left(\frac{GM_{\text{CMK}}}{a_f} - \frac{GM_i M_{\text{K}}}{a_i} \right) = |E_{\text{bind}}|, \quad (3)$$

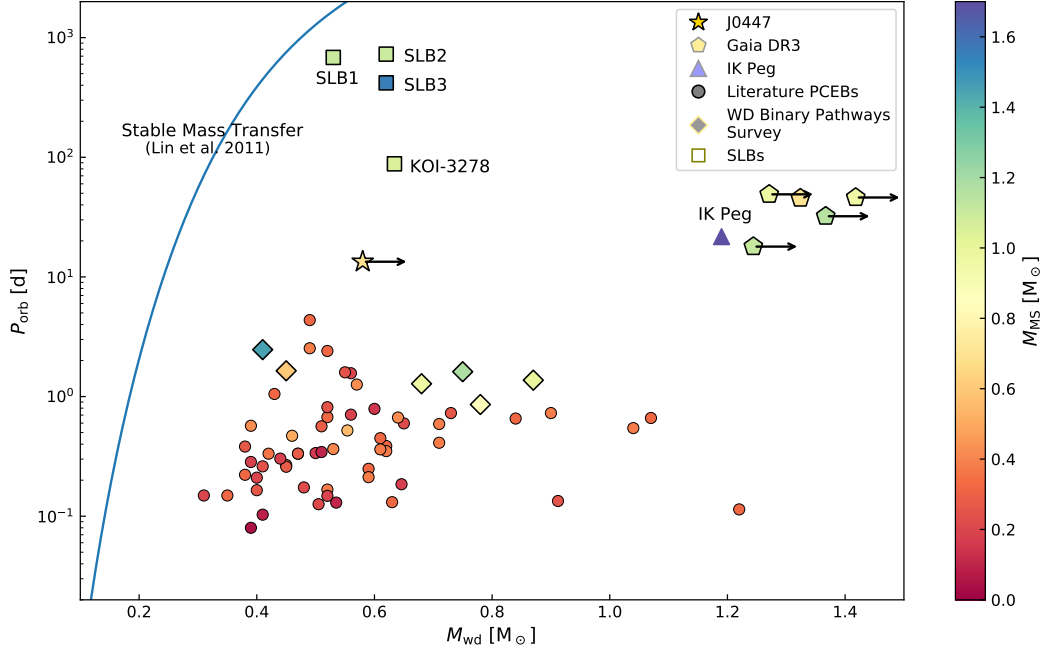


Figure 8. Orbital period versus WD mass distribution of PCEBs, including J0447 system presented in this work. The blue line shows the theoretical $M_{\text{wd}}-P_{\text{orb}}$ relation for the stable mass transfer case by Lin et al. (2011). A large number PCEBs with M-dwarf companion (circle markers) compiled by Zorotovic et al. (2010) exhibits an orbital period distribution concentrated below 10 days. The six PCEB systems from the ‘White Dwarf Binary Pathways Survey’ are denoted by diamond markers (Hernandez et al. 2021, 2022a,b). The pentagon and triangle markers denote five PCEBs hosting massive white dwarf binary candidates from *Gaia* DR3 (Yamaguchi et al. 2024) and IK Peg, respectively. These systems are distinguished from other known PCEBs by their long orbital periods. The KIC 8145441 system (Kruse & Agol 2014) and other SLBs (Kawahara et al. 2018), indicated by square markers, were all detected by Kepler.

$$E_{\text{bind}} = \int_{M_c}^{M_i} \left(-\frac{Gm}{r} + \varepsilon_{\text{int}} \right) dm, \quad (4)$$

where G is the gravitational constant; M_C and M_K are the masses of the compact object and companion star, respectively; a_i and a_f are the binary separation at the onset of CE and after the ejection of CE, M_i is the progenitor mass of the compact object, M_c is its core mass at the onset of CE and α_{CE} is the CE efficiency. E_{bind} is the binding energy of the envelope of the progenitor of the WD. m is the mass coordinate, r is the radius and ε_{int} is the internal energy, which includes the radiation energy and thermal energy, but not the recombination energies.

In order to obtain the binding energy of the progenitors of WDs, we compute a grid of single stellar evolution models with the stellar evolution code Modules for Experiments in Stellar Astrophysics (MESA, Paxton et al. 2011, 2013, 2015, 2018, 2019). The initial stellar mass ranges from $1.0 M_{\odot}$ to $8 M_{\odot}$ with a step of $0.50 M_{\odot}$. The initial chemical abundances are assumed to be $X = 0.73$, $Y = 0.26$, $Z = 0.01$. The mixing length parameter is assumed to be 2.0 and overshooting is not considered in our calculation. Regarding the stellar wind, we adopt the prescription of Reimers (1975) with a wind efficiency parameter of 0.5 for RG stars and the prescription of Bloecker (1995) with a wind efficiency parameter of 0.10 for AGB stars. The stars are evolved from zero-age MS to WD phase. In Fig. 9, we show an example of the single stellar evolution track in our calculation. The initial mass in that plot is $1.5 M_{\odot}$.

We constrain the WD mass to be within the range of $0.56 - 1.40 M_{\odot}$ and α_{CE} within 0-1.0. Then we can constrain the progenitor mass of the WD and also the initial orbital period, which are shown in Fig. 10. From this plot, we can find that the progenitor mass of the WD is around $1.5 - 8.0 M_{\odot}$ and the initial orbital period is around $340 - 4200$ days.

5. CONCLUSIONS

We report an SB1 that contains a K-type star and a compact object in the solar neighborhood. Although the nature of a compact object has not yet been determined, this binary system is likely a PCEB consisting of WD and

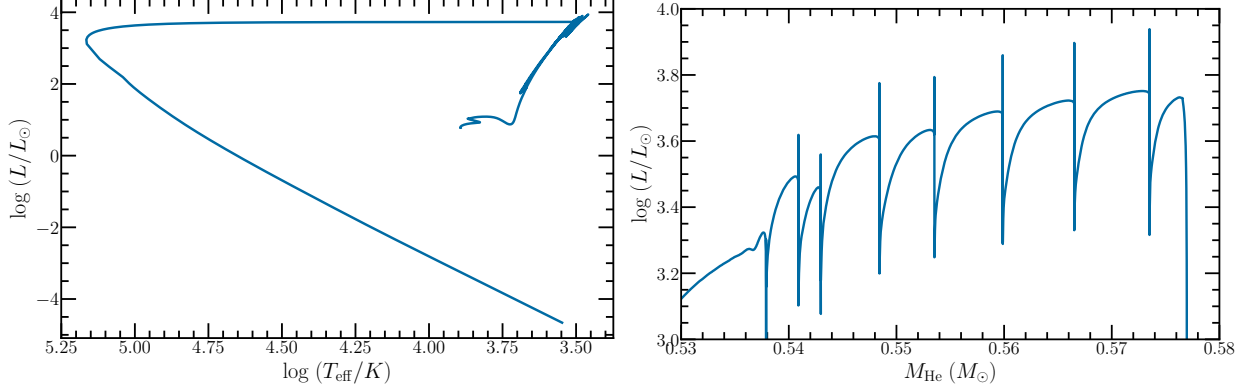


Figure 9. Left panel: evolution of a $1.5 M_{\odot}$ star in the HR diagram; Right panel: evolution of luminosity as a function of He core mass around the TP-AGB phase for a $1.5 M_{\odot}$ star.

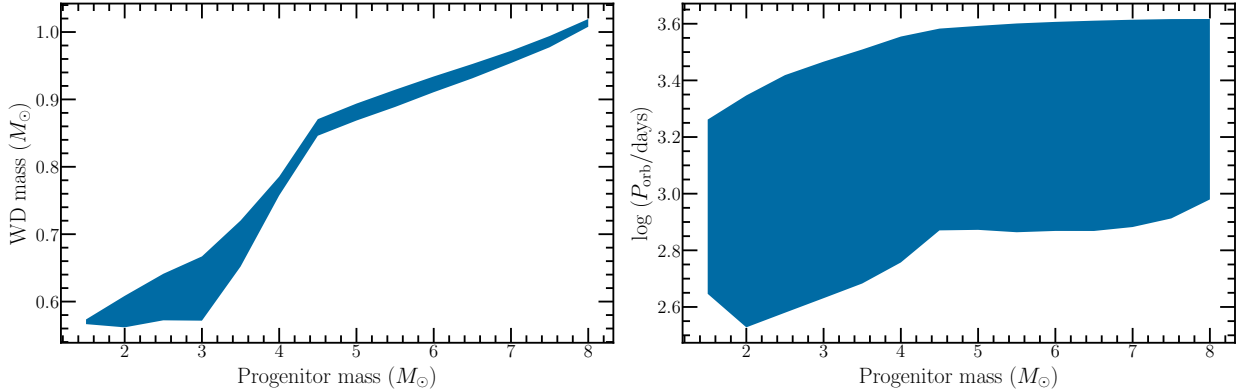


Figure 10. The initial binary parameter space of the progenitors of J0447 in the WD mass versus its progenitor mass panel and progenitor mass versus initial orbital period panel.

K-type companions with intermediate orbital periods between tight and wide orbital periods. If the compact object is a BH, it will be the nearest BH, which may help us to understand the origin of radionuclide element in the solar neighborhood. However, analyses based on machine-learning techniques applied to low-resolution spectra indicate a potential overabundance of *s*-process elements in the K-type star, which further supports that the compact object is a WD. Furthermore, considering the relatively low inclination probability presented in section 4.2, an NS or BH companion is a less likely scenario. For a PCEB with intermediate orbital periods, we found that extra energy is not required to explain this system when the WD progenitors experienced a highly evolved TP-AGB phase at the onset of the CE evolution. Importantly, the K-type companion, a potential Barium star candidate, shows overabundance of heavy elements heavier than iron produced by the *s*-process. This is because the material formed in the interior of the more evolved WD progenitor being transferred onto the companion star. This system provides insight into the efficiency of CE ejection and suggests that additional energy sources are not required to expel the envelope during the CEE. Nevertheless, high-resolution spectroscopy observations are crucial to verify the *s*-process overabundance in the K-type companion and to test for a possible misclassification as a barium star. If the K-type companion star is confirmed to be a barium star, this would represent the shortest orbital period barium star binary system discovered to date, which may hold significant implications for understanding the formation and evolution of barium star binary systems.

ACKNOWLEDGMENTS

We thank Dr. Weimin Gu, Dr. Smith, D. A, and Dr. Lin Lan for their helpful discussions. The Guoshoujing Telescope (the Large Sky Area Multi-Object Fiber Spectroscopic Telescope, LAMOST) is a National Major Scientific Project built by the Chinese Academy of Sciences. Funding for the project has been provided by the National Development and Reform Commission. LAMOST is operated and managed by the National Astronomical Observatories, Chinese Academy of Sciences. FAST is a Chinese national mega-science facility, operated by the National Astronomical Observatories, Chinese Academy of Sciences. ZTF is a public-private partnership, with equal support from the ZTF Partnership and from the U.S. National Science Foundation through the Mid-Scale Innovations Program (MSIP). J.L. acknowledges the support of the Postdoctoral Fellowship Program of CPSF under Grant Number GZC20240905. Y. L. acknowledges the support of the Boya fellowship of Peking University and the China Postdoctoral Science Foundation (No. 2025T180924). H. L. acknowledges the support of the CAS "Light of West China", the Young Talent Project of Yunnan Revitalization Talent Support Program, the Yunnan Fundamental Research Project (No. 202401BC070007). This work is supported by the National Natural Science Foundation of China under grant 12403055, 12221003, 12335009, 12288102, 12333008 and 12422305.

REFERENCES

Abazajian, K. N., Adelman-McCarthy, J. K., Agüeros, M. A., et al. 2009, *ApJS*, 182, 2, 543.
doi:10.1088/0067-0049/182/2/543

Abdollahi, S., Acero, F., Baldini, L., et al. 2022, *ApJS*, 260, 53. doi:10.3847/1538-4365/ac6751

Blaauw, A. 1961, *BAN*, 15, 265.

Bloecker, T. 1995, *A&A*, 297, 727.

Binns, W. R., Israel, M. H., Christian, E. R., et al. 2016, *Science*, 352, 6286, 677. doi:10.1126/science.aad6004

Blanco-Cuaresma, S., Soubiran, C., Heiter, U., et al. 2014, *A&A*, 569, A111. doi:10.1051/0004-6361/201423945

Blanco-Cuaresma, S. 2019, *MNRAS*, 486, 2075.
doi:10.1093/mnras/stz549

Belloni, D., Schreiber, M. R., & Zorotovic, M. 2024, *A&A*, 687, A12. doi:10.1051/0004-6361/202449320

Bhattacharya, D. & van den Heuvel, E. P. J. 1991, *PhR*, 203, 1-2, 1. doi:10.1016/0370-1573(91)90064-S

Belczynski, K., Holz, D. E., Bulik, T., et al. 2016, *Nature*, 534, 7608, 512. doi:10.1038/nature18322

De, K., Kasliwal, M. M., Ofek, E. O., et al. 2018, *Science*, 362, 6411, 201. doi:10.1126/science.aas8693

Davis, P. J., Kolb, U., & Willems, B. 2010, *MNRAS*, 403, 1, 179. doi:10.1111/j.1365-2966.2009.16138.x

Escorza, A. & De Rosa, R. J. 2023, *A&A*, 671, A97.
doi:10.1051/0004-6361/202244782

Fimiani, L., Cook, D. L., Faestermann, T., et al. 2016, *PhRvL*, 116, 15, 151104.
doi:10.1103/PhysRevLett.116.151104

Gustafsson, B., Edvardsson, B., Eriksson, K., et al. 2008, *A&A*, 486, 951. doi:10.1051/0004-6361:200809724

Gaia Collaboration, Arenou, F., Babusiaux, C., et al. 2023, *A&A*, 674, A34. doi:10.1051/0004-6361/202243782

Green, G. M., Schlafly, E., Zucker, C., et al. 2019, *ApJ*, 887, 93. doi:10.3847/1538-4357/ab5362

Gaia Collaboration, Panuzzo, P., Mazeh, T., et al. 2024, *A&A*, 686, L2. doi:10.1051/0004-6361/202449763

Hernandez, M. S., Schreiber, M. R., Parsons, S. G., et al. 2021, *MNRAS*, 501, 2, 1677. doi:10.1093/mnras/staa3815

Hernandez, M. S., Schreiber, M. R., Parsons, S. G., et al. 2022a, *MNRAS*, 517, 2, 2867.
doi:10.1093/mnras/stac2837

Hernandez, M. S., Schreiber, M. R., Parsons, S. G., et al. 2022b, *MNRAS*, 512, 2, 1843. doi:10.1093/mnras/stac604

Hurley, J. R., Tout, C. A., & Pols, O. R. 2002, *MNRAS*, 329, 4, 897. doi:10.1046/j.1365-8711.2002.05038.x

Iben, I. & Tutukov, A. V. 1986, *ApJ*, 311, 742.
doi:10.1086/164812

Iben, I. & Livio, M. 1993, *PASP*, 105, 1373.
doi:10.1086/133321

Jiang, P., Tang, N.-Y., Hou, L.-G., et al. 2020, *Research in Astronomy and Astrophysics*, 20, 5, 064.
doi:10.1088/1674-4527/20/5/64

Koll, D., Korschinek, G., Faestermann, T., et al. 2019, *PhRvL*, 123, 7, 072701.
doi:10.1103/PhysRevLett.123.072701

Knie, K., Korschinek, G., Faestermann, T., et al. 1999, *PhRvL*, 83, 1, 18. doi:10.1103/PhysRevLett.83.18

Kruse, E. & Agol, E. 2014, *Science*, 344, 6181, 275.
doi:10.1126/science.1251999

Kawahara, H., Masuda, K., MacLeod, M., et al. 2018, *AJ*, 155, 3, 144. doi:10.3847/1538-3881/aaaaaf

Kalogera, V. & Webbink, R. F. 1998, *ApJ*, 493, 1, 351.
doi:10.1086/305085

El-Badry, K., Rix, H.-W., Cendes, Y., et al. 2023, *MNRAS*, 521, 3, 4323. doi:10.1093/mnras/stad799

El-Badry, K., Rix, H.-W., Quataert, E., et al. 2023, MNRAS, 518, 1, 1057. doi:10.1093/mnras/stac3140

Lomb, N. R. 1976, Ap&SS, 39, 447. doi:10.1007/BF00648343

Lin, J., Li, C., Wang, W., et al. 2023, ApJL, 944, L4. doi:10.3847/2041-8213/acb54b

Lin, J., Chen, H., Wang, B., et al. 2024, ApJL, 960, 1, L5. doi:10.3847/2041-8213/ad1580

Lin, J., Rappaport, S., Podsiadlowski, P., et al. 2011, ApJ, 732, 2, 70. doi:10.1088/0004-637X/732/2/70

Luo, A.-L., Zhao, Y.-H., Zhao, G., et al. 2015, Research in Astronomy and Astrophysics, 15, 8, 1095. doi:10.1088/1674-4527/15/8/002

Liu, H.-B., Gu, W.-M., Zhang, Z.-X., et al. 2024, ApJ, 969, 2, 114. doi:10.3847/1538-4357/ad4c6f

McClure, R. D., Fletcher, J. M., & Nemec, J. M. 1980, ApJL, 238, L35. doi:10.1086/183252

Mann, A. W., Dupuy, T., Kraus, A. L., et al. 2019, ApJ, 871, 63. doi:10.3847/1538-4357/aaf3bc

Men, Y. & Barr, E. 2024, A&A, 683, A183. doi:10.1051/0004-6361/202348247

Price-Whelan, A. M., Hogg, D. W., Foreman-Mackey, D., et al. 2017, ApJ, 837, 20. doi:10.3847/1538-4357/aa5e50

Price-Whelan, A. M. 2017, The Journal of Open Source Software, 2, 388. doi:10.21105/joss.00388

Piskunov, N. & Valenti, J. A. 2017, A&A, 597, A16. doi:10.1051/0004-6361/201629124

Paczynski, B. 1976, Structure and Evolution of Close Binary Systems, 73, 75.

Paxton, B., Smolec, R., Schwab, J., et al. 2019, ApJS, 243, 1, 10. doi:10.3847/1538-4365/ab2241

Paxton, B., Schwab, J., Bauer, E. B., et al. 2018, ApJS, 234, 2, 34. doi:10.3847/1538-4365/aaa5a8

Paxton, B., Marchant, P., Schwab, J., et al. 2015, ApJS, 220, 1, 15. doi:10.1088/0067-0049/220/1/15

Paxton, B., Cantiello, M., Arras, P., et al. 2013, ApJS, 208, 1, 4. doi:10.1088/0067-0049/208/1/4

Paxton, B., Bildsten, L., Dotter, A., et al. 2011, ApJS, 192, 1, 3. doi:10.1088/0067-0049/192/1/3

Qi, S., Gu, W.-M., Yi, T., et al. 2023, AJ, 165, 5, 187. doi:10.3847/1538-3881/acc389

Scargle, J. D. 1982, ApJ, 263, 835. doi:10.1086/160554

Song, S., Kong, X., Bu, Y., et al. 2024, ApJ, 974, 1, 78. doi:10.3847/1538-4357/ad6b2c

Reimers, D. 1975, Memoires of the Societe Royale des Sciences de Liege, 8, 369.

Ransom, S. M. 2001, Ph.D. Thesis, Harvard University, Massachusetts.

Rebassa-Mansergas, A., Gänsicke, B. T., Rodríguez-Gil, P., et al. 2007, MNRAS, 382, 4, 1377. doi:10.1111/j.1365-2966.2007.12288.x

Ren, J.-J., Raddi, R., Rebassa-Mansergas, A., et al. 2020, ApJ, 905, 1, 38. doi:10.3847/1538-4357/abc017

Vines, J. I. & Jenkins, J. S. 2022, MNRAS, 513, 2719. doi:10.1093/mnras/stac956

Wu, Q. D., Yuan, J. P., Wang, N., et al. 2023, MNRAS, 522, 4, 5152. doi:10.1093/mnras/stad1323

Wallner, A., Feige, J., Kinoshita, N., et al. 2016, Nature, 532, 7597, 69. doi:10.1038/nature17196

Warner, B. 1995, , 28.

Webbink, R. F. 1984, ApJ, 277, 355. doi:10.1086/161701

Wonnacott, D., Kellett, B. J., & Stickland, D. J. 1993, MNRAS, 262, 277. doi:10.1093/mnras/262.2.277

Xiang, M., Ting, Y.-S., Rix, H.-W., et al. 2019, ApJS, 245, 2, 34. doi:10.3847/1538-4365/ab5364

Yuan, H., Wang, S., Bai, Z., et al. 2022, ApJ, 940, 165. doi:10.3847/1538-4357/ac9c62

Yamaguchi, N., El-Badry, K., Fuller, J., et al. 2024, MNRAS, 527, 4, 11719. doi:10.1093/mnras/stad4005

Yao, Y., De, K., Kasliwal, M. M., et al. 2020, ApJ, 900, 1, 46. doi:10.3847/1538-4357/abaa3d

Yao, J. M., Manchester, R. N., & Wang, N. 2017, ApJ, 835, 1, 29. doi:10.3847/1538-4357/835/1/29

Yi, T., Gu, W.-M., Zhang, Z.-X., et al. 2022, Nature Astronomy, 6, 1203. doi:10.1038/s41550-022-01766-0

Zorotovic, M., Schreiber, M. R., Gänsicke, B. T., et al. 2010, A&A, 520, A86. doi:10.1051/0004-6361/200913658

Zheng, L.-L., Gu, W.-M., Sun, M., et al. 2022, ApJ, 936, 1, 33. doi:10.3847/1538-4357/ac853f

Zhao, X., Mu, H., Wang, S., et al. 2024, ApJ, 964, 1, 101. doi:10.3847/1538-4357/aced95

Zhang, M., Xiang, M., Ting, Y.-S., et al. 2025, ApJS, 279, 1, 5. doi:10.3847/1538-4365/add016